JP1.12

CLOUD MASK AND QUALITY CONTROL FOR SST WITHIN THE ADVANCED CLEAR SKY PROCESSOR FOR OCEANS (ACSPO)

B. Petrenko*[1,2], A. Ignatov[1], N. Shabanov[1,2], X. Liang[3], Y. Kihai[4], A. Heidinger[5]

[1]NOAA/NESDIS, Center for Satellite Applications and Research (STAR), Camp Springs, Maryland
[2]IMSG Inc., Kensington, Maryland
[3]Cooperative Institute for Research in the Atmospheres (CIRA), Fort Collins, Colorado
[3]Perot Systems Government Services, Lanham, Maryland
[5]NOAA/NESDIS, Madison, Wisconsin

1. INTRODUCTION

The Advanced Clear Sky Processor for Oceans (ACSPO), newly developed at NESDIS, will enhance clear-sky ocean products, such as clear-sky radiances (CSR), sea surface temperatures (SST), T_S, and aerosols, generated from measurements in the atmospheric transparency windows in visible (VIS), near infrared (NIR), and thermal infrared (TIR) spectral ranges. Initially, ACSPO was developed to replace the operational Main Unit Task (MUT) system, currently processing data of the Advanced Very High Resolution Radiometer (AVHRR) (McClain et al., 1985; Ignatov et al., 2004). Recently the scope of ACSPO applications has been extended to Meteosat Second Generation-Spinning Enhanced Visible and Infrared Imager (MSG SEVIRI) (Shabanov et al., 2009). Other potential ACSPO applications include generation of clear-sky ocean products from the Visible Infrared Imager Radiometer Suite (VIIRS) onboard the National Polar-orbiting Operational Environmental Satellite System (NPOESS) and Advanced Baseline Imager (ABI) onboard GOES-R.

This paper describes the ACSPO cloud-masking algorithm as it applies to AVHRR data processing. The AVHRR/3 instrument, flown onboard the NOAA-KLMN and MetOp satellites, measures the top of the atmosphere reflectances in three solar reflectance bands centered at 0.63 μm (Ch1), 0.83 μm (Ch2), and 1.61 μm (Ch3A), as well as three brightness temperatures (BT) in three Earth emission bands centered at 3.7 μm (Ch3B), 10.8 μm (Ch4), and 12 μm (Ch5). Ch3A is now time-shared with Ch3B as only the 3A or 3B band can be transmitted, according to the logic reprogrammable from Earth. For instance, on the morning satellites NOAA-17 and MetOp-A Ch3B is "on" (and hence Ch3A is "off") on the dark side of the Earth, whereas on the sunlit part of the orbit, these positions are switched over automatically to a "Ch3A on/Ch3B off" mode (NOAA KLM User's Guide, 2003). On the afternoon satellites NOAA-16 and -18, Ch3B is on all the time, per a request from the fire community. The AVHRR data are available in two formats with different spatial resolutions. In the Global Area Coverage (GAC) format, the AVHRR scan is comprised of 409 fields of view (pixels) of 4 km size at nadir. In the Local Area Coverage mode (LAC) and in the Full Resolution Area Coverage format (FRAC, enabled on MetOp-A), every scan includes 2048 pixels of 1 km size at nadir.

The goal of the ACSPO cloud-masking algorithm is to detect the pixels, contaminated with clouds, while preserving for the further analyses as many clear-sky pixels as possible. Approaching optimality in the above sense requires close consideration of cloud effects on the specific clear-sky products (e.g., Cayula and Cornillon, 1996; Martins et al., 2002; Pellegrini et al., 2006).

ACSPO adopts the most common approach to cloud masking, which implies classification of pixels into a few categories from "clear" to "cloudy" based on comparisons of cloud predictors constructed from observed radiances against predefined thresholds. In general, thresholds for cloud tests are selected from clear-sky radiative transfer simulations based on reference fields of ocean and atmospheric variables. For predictors derived from infrared BTs, the most important variables are SST, atmospheric water vapor, and temperature profiles. The information about these variables can be available in the form of either static (climate) or dynamic (Numerical Weather Prediction, or NWP) data. The use of static reference fields (e.g., Saunders and Kriebel, 1988; Stowe et al., 1999) makes the algorithm more stable and insensitive with respect to the missing external ancillary information. The use of NWP reference fields (e.g., Derrien and Le Gleau, 2005; Dybbroe et al., 2005; Minnis et al., 2008) allows more accurate specification of the thresholds. In ACSPO this dilemma is resolved by including two modules, ACSPO Cloud Mask (ACM) and ACSPO Quality Control (AQC), which emphasize different combinations of stability and accuracy. While ACM uses only static thresholds, AQC provides more accurate cloud filtering using dynamic fields of SST and water vapor. On-line radiative transfer simulations for AQC are enabled with the fast Community Radiative Transfer Model (CRTM) (Han et al., 2005), which is incorporated in ACSPO (Liang et al., 2009).

* *Corresponding author address*: Boris Petrenko, WWB, Rm. 601, 5200 Auth Rd., Camp Springs, MD 20746-4304; e-mail: Boris.Petrenko@noaa.gov

Both in ACM and AQC, the retrieved SST, T_S, plays an important role as a cloud predictor. This is not an ACSPO novelty. T_S has been used among other cloud predictors in many cloud masking algorithms such as Derrien and Le Gleau (2005), Dybbroe et al. (2005), and Heidinger (2004), to name a few. In some algorithms aimed specifically at SST retrievals (Cayula and Cornillon, 1996; Pellegrini et al., 2006), T_S is the only cloud predictor. Like many other cloud predictors, T_S is calculated as a linear combination of measured BTs. However, using T_S takes several important advantages for cloud masking. First, T_S is supported with the most detailed *a priori* information in the form of both climate and NWP reference fields. Second, this BT combination is designed to minimize sensitivity to the global atmospheric water vapor variations, thus allowing direct comparison against the reference SST field, without correction for atmospheric absorption or RTM simulations. Third, the use of T_S as a cloud predictor directly addresses cloud contamination within the product. However, in order to fully exploit these advantages, real characteristics of accuracy of both T_S and reference SST fields should be taken into account.

2. THE HISTORY OF ACSPO CLOUD MASK

ACSPO builds upon the latest version of the Clouds From AVHRR Extended Algorithm (CLAVRx) (Heidinger et al., 2002; Heidinger, 2004), which traces back to CLAVR-1 (Stowe et al., 1999), which in turn has grown out of the MUT. The focus of CLAVRx has been on cloud detection and typing both over sea and land at a pixel resolution. Since the task of ACSPO cloud masking is different from one of CLAVRx, the ACSPO cloud-masking algorithm has significantly departed from its predecessor. ACSPO version 1.0, which became operational in May 2008 with AVHRR GAC data from NOAA-18 and MetOp-A, included a single cloud-masking module, the ACSPO Clear-Sky Mask (ACSM) (Petrenko et al., 2008; Liang et al., 2009). The ACSM included both ACM and AQC tests and, among others, the SST test, which compared T_S against the 1° Weekly Optimum Interpolated SST version 2 (OI.v2, Reynolds et al., 2002). ACSPO version 1.0 also forms the basis of the current cloud mask for MSG SEVIRI, used as a prototype for GOES-R ABI (Shabanov et al., 2009). In the next ACSPO version 1.1, which is currently becoming operational with AVHRR data, the weekly OI.v2 SST has been replaced with more accurate 0.25° Daily High-Resolution-Blended SST (Reynolds et al., 2007). Another improvement over version 1.0 has been accounting for T_S bias, induced by the regression SST retrieval algorithm. This algorithm-induced bias had a remarkable impact on ACSM pixel classification and caused variations in clear-sky statistics of T_S anomalies, observed with AVHRR from different satellites. Separation of the ACSPO cloud tests into ACM and AQC, which is discussed in this paper, has been initiated by the requirement of the GOES-R Algorithm Working Group to provide the cloud-masking module upstream the product retrieval modules. It has been prototyped with AVHRR data and is planned for implementation within future ACSPO versions for AVHRR and GOES-R ABI.

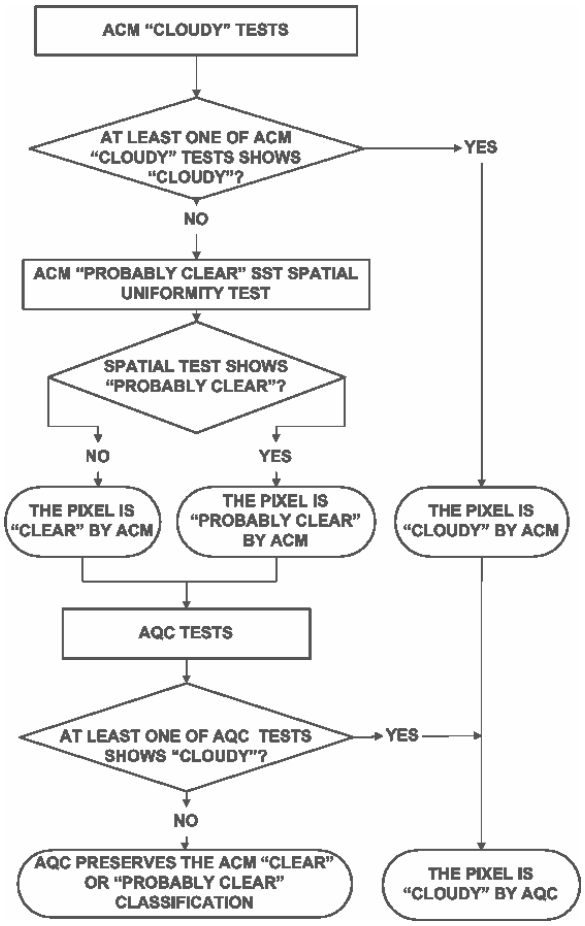

Fig. 1. The flow chart of ACM and AQC.

3. THE FLOW CHART OF ACM AND AQC

Fig. 1 shows the joint flow chart of ACM and AQC. ACM classifies AVHRR pixels over ocean into three categories: "clear", "probably clear", and "cloudy". The "probably cloudy" category available in CLAVRx was omitted in ACSPO, which is a clear-sky application and therefore only requires information on whether the pixel is usable or unusable for SST. The "probably usable" category was kept for users with less stringent quantitative requirements to SST.

The pixel is classified as "cloudy" if it fails to pass at least one out of five cloudy tests. The group of ACM cloudy tests includes an SST test, spectral BT test, and three daytime reflectance tests. The ACM SST test compares T_S against 1° monthly climate SST (e.g., Xue et al., 2003). It first classifies the pixels by detecting unrealistically cold T_S anomalies with respect to the monthly climate SST field and then refines this classification, analyzing statistics of "clear" and "cloudy"

pixels within sliding windows surrounding tested pixels. The spectral BT test adopts the CLAVRx "four minus five" test (FMFT) for the daytime and "three minus five" test (TMFT) for the nighttime. The thresholds for the spectral BT test have been redefined to minimize multiple false cloud detections, observed in CLAVRx (Petrenko et al., 2008). The pixels, which pass all ACM "cloudy" tests, are preliminarily classified as "clear". They are subsequently tested with the SST spatial uniformity test, which detects fractional and semitransparent cloudiness by elevated spatial variability of T_S and reclassifies some "clear" pixels into "probably clear". The reflectance tests, including the reflectance gross contrast test (RGCT), reflectance ratio contrast test (RRCT), and Channel 3 albedo test (C3AT), are adopted from CLAVRx without changes.

The pixels classified as "cloudy" by ACM are not further processed with AQC. The pixels classified as "clear" and "probably clear" are passed on to AQC, which can reclassify some of them into "cloudy".

The AQC differs from the ACM in that it uses current and more accurate data on the SST and atmosphere (rather than their climatologic first guesses in the ACM) in conjunction with real-time CRTM calculations. For atmosphere, it is the National Centers for Environmental Prediction (NCEP) Global Forecast System 6hr 1° upper air fields (http://nomad3.ncep.noaa.gov/pub/gfs/rotating/). The AQC SST test uses the same logic as the ACM SST test, but applies it to T_S anomalies with respect to Daily High-Resolution-Blended Reynolds SST. The AQC BT test verifies the quality of approximation of observed BTs against clear-sky BTs, simulated with CRTM from T_S and NCEP water vapor atmospheric profiles. If the pixel has passed through both AQC tests, then it retains the classification assigned by the ACM; otherwise, it is reclassified as "cloudy".

4. ESTIMATION OF THE ALGORITHM-INDUCED T_S BIASES

Currently, ACSPO retrieves SST using regression algorithms (McClain et al., 1985). During daytime the split-window nonlinear SST (NLSST) algorithm is used:

$$T_S = a_0+a_1T_4+a_2T_{REF}(T_4-T_5)+a_3(T_4-T_5)(\sec\theta-1) \quad (1)$$

During nighttime, the multi-channel SST (MCSST) algorithm is used:

$$T_S = b_0+b_1T_{3b}+b_2T_4+b_3T_5+[b_4(T_{3b}-T_5)+b_5](\sec\theta-1) \quad (2)$$

Here, T_{3b}, T_4, and T_5 are observed BTs in the AVHRR channels 3b, 4, and 5; θ is the view zenith angle; a_0, a_1, a_2 a_3, and b_0, b_1, b_2, b_3, b_4, and b_5 are coefficients derived from regression of observed BTs against *in situ* SST measurements, and T_{REF} is SST taken from the reference data set. For ACM, the reference SST field, T_C, is obtained by interpolation of 1° monthly climate SST to AVHRR pixel, whereas for AQC the reference SST field, T_A, is obtained by interpolation of the global SST analysis (in ACSPO v.1.10, it is 0.25° Daily Reynolds SST).

For AVHRR data processing, ACSPO currently adopts the formulations and coefficients for the regression SST from the MUT system without change. These regression SST estimates may be biased with respect to *in situ* SST. The biases of equations (1) and (2) can change in time due to satellite sensor calibration instabilities or orbital drift. These algorithm-induced biases in satellite SSTs with respect to *in situ* SST are accounted for in the production of Reynolds SST data set (e.g., Reynolds et al., 2007), and they should also be taken into account in the cloud test that compares T_S against reference SST field. Within ACSPO the T_S biases with respect to T_C and T_A, B_C and B_A, are estimated dynamically from histograms of (T_S-T_C) and (T_S-T_A) anomalies, accumulated over all ocean pixels using an approximately 24-hour sliding window preceding the time of observations.

Because daytime and nighttime T_S are produced with different expressions (1) and (2) and SST is subject to diurnal variability, the biases are monitored separately for day and night. Figs. 2 and 3 show the day- and nighttime anomaly histograms for four platforms. The histograms were accumulated over 100 orbits of each platform from August 1 to 7, 2008. Although the fraction of clear-sky pixels over ocean is typically only 15 to 20%, the clear-sky T_S anomalies are concentrated within a relatively narrow range and form well-defined histogram maxima. The T_S anomaly values, at which the maxima take place, vary between the platforms. The locations of histogram maxima on the T_S anomaly axis are taken as estimates of algorithm-induced biases. Fig. 4 shows B_A for four platforms as functions of the orbit number.

5. THE ACM TESTS

5.1 *The ACM SST Test*

The predictor for the ACM SST test is the anomaly of T_S with respect to T_C, corrected for the algorithm-induced bias:

$$\Delta T_C = T_S - T_C - B_C \quad (3)$$

The test is applied to the ΔT_C field in two steps. On the first step, obviously unrealistic negative anomalies are screened out with the following condition:

$$\Delta T_C < \Delta T_{ACM\ SST}? \quad (4)$$

If yes, then the pixel is set to "cloudy"; otherwise, it is set to "clear" The threshold $\Delta T_{ACM\ SST}$ is set to a conservative static value of -6K. This value was defined from a comparison of T_A and T_C fields for the time period of August 1 to 7, 2008. Fig. 5 shows a composite map of minimum differences between T_C and T_A. For the vast majority of the world ocean, this minimum difference is greater than –6 K. Fig. 6 shows a cumulative distribution of T_A-T_C. According to Fig. 6, the difference T_A - T_C is less than –6 K for no more than 0.0001% of ocean pixels.

Next, the adaptive part of the SST test specifies the initial pixel classification based on the analysis of T_S

anomaly statistics in "clear" and "cloudy" clusters within a sliding window, surrounding the tested pixel. The size of the sliding window was chosen to be 31 × 31 GAC pixels. All "clear" pixels within the window are tested with the following condition:

$$|\Delta T_C - \Delta T_{CLOUD}|/\sigma_{CLOUD} < |\Delta T_C|/\sigma_{CLEAR}? \quad (5)$$

If yes, then the pixel is "cloudy". In (4), ΔT_{CLOUD} and σ_{CLOUD} are mean and STD of ΔT_C over all "cloudy" pixels within the sliding window, and

$$\sigma_{CLEAR} = \Delta T_{ACM\ SST}/3. \quad (6)$$

The procedure repeats itself until either the classification of the pixels within the window stabilizes or the tested (central) pixel in the window becomes "cloudy".

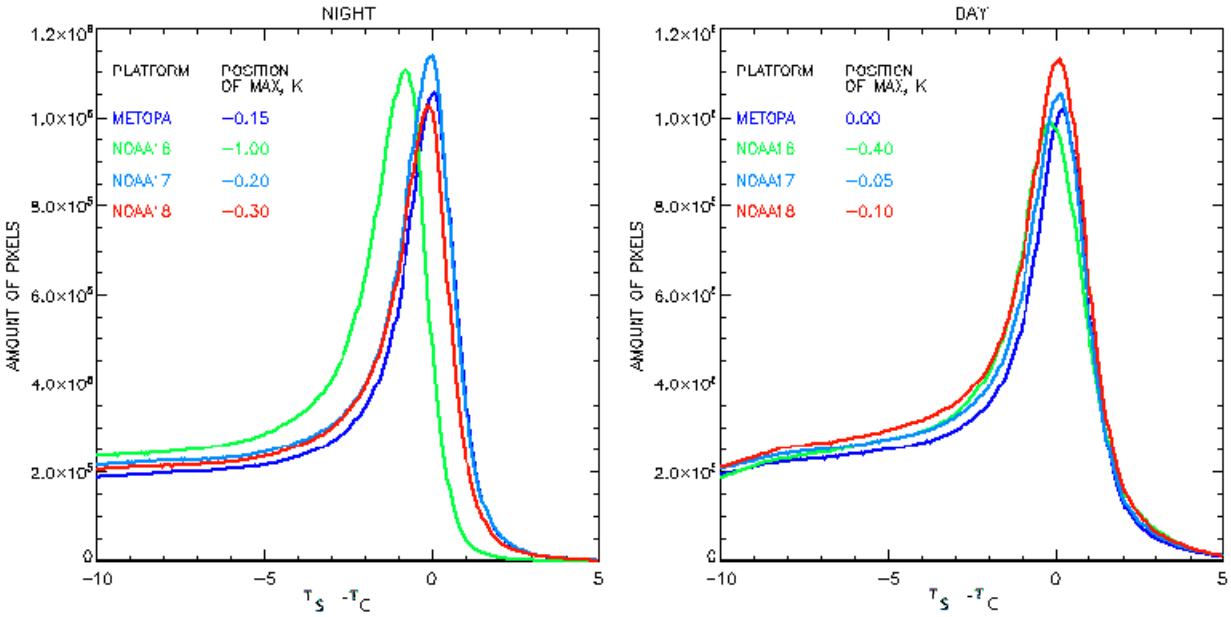

Fig. 2. Histograms of T_S - T_C anomalies over all ocean pixels for August 1 to 7, 2008 for four platforms. Positions of histogram maxima are defined as the most populated 0.05 K bin and shown on the top of each plot.

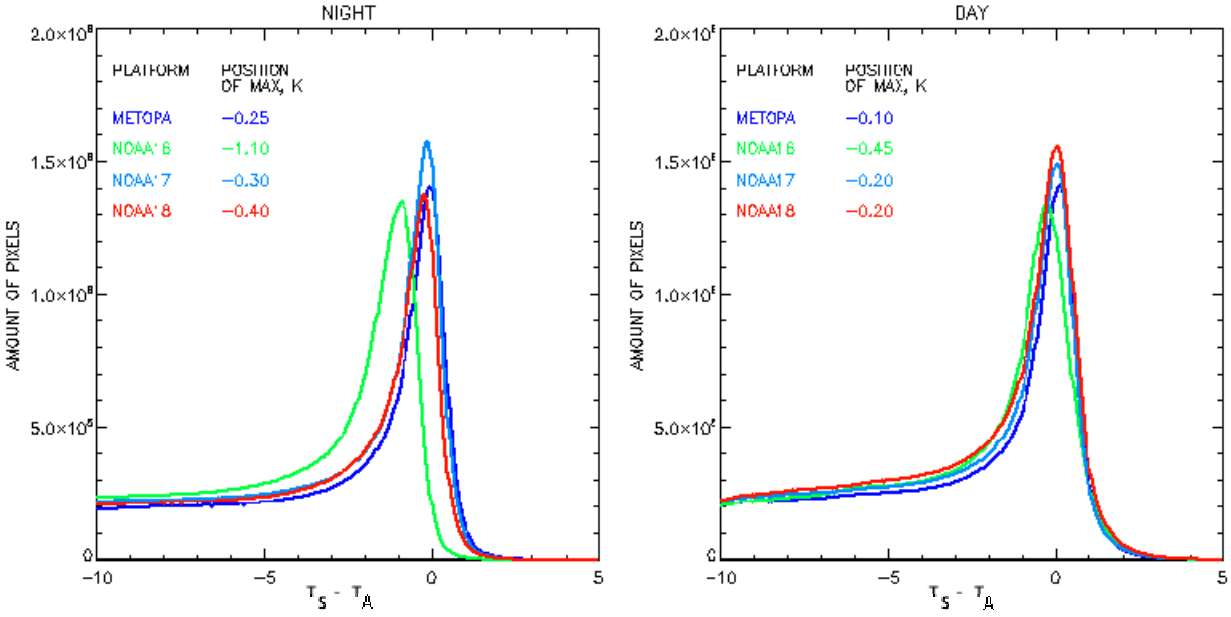

Fig. 3. Histograms of T_S - T_A anomalies over all ocean pixels for August 1 to 7, 2008 for four platforms. Positions of histogram maxima are defined as the most populated 0.05 K bin and shown on the top of each plot.

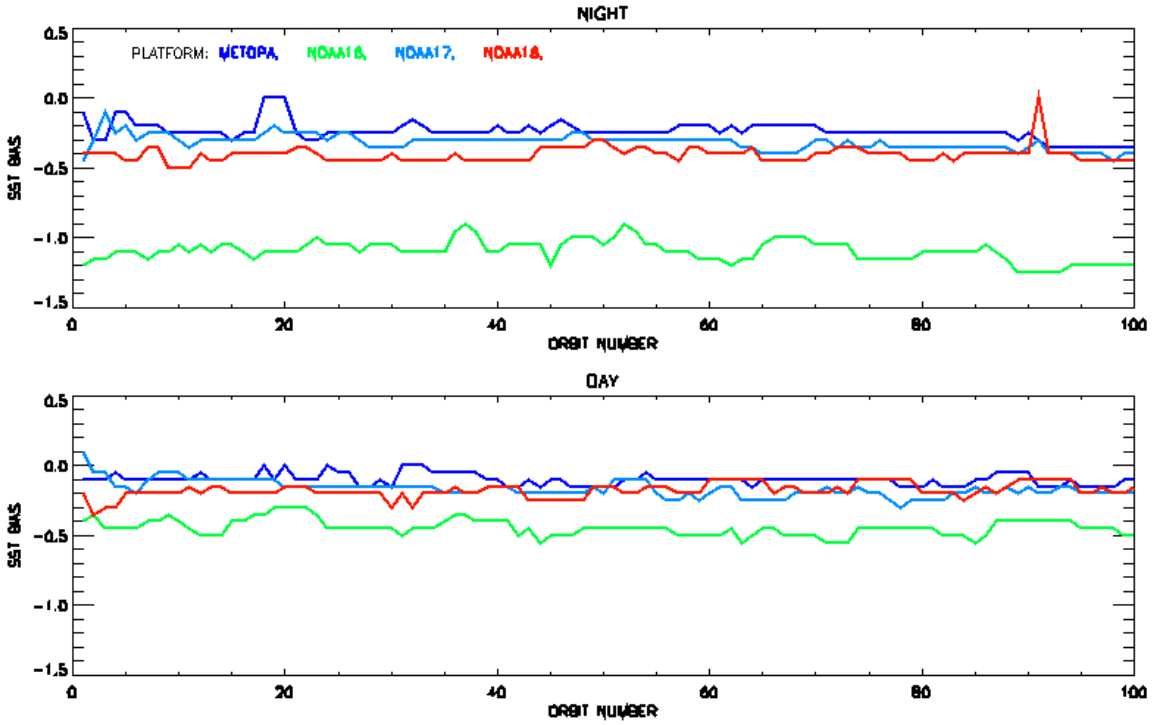

Fig. 4. The algorithm-induced biases B_A for four platforms from August 1 to 7, 2008 as a function of orbit number.

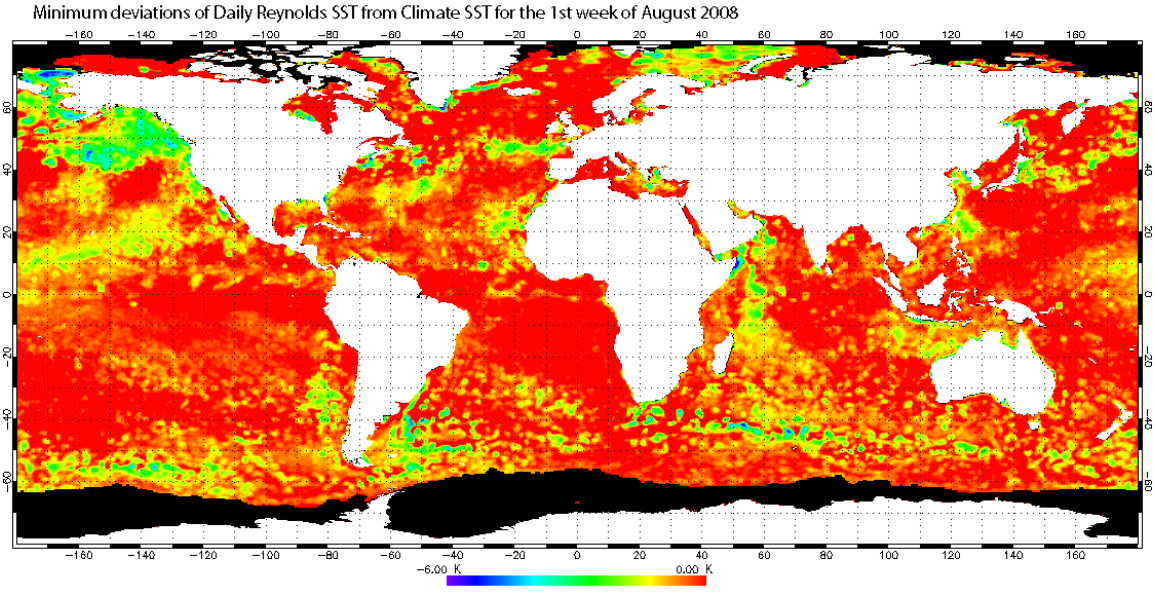

Fig. 5. The distribution of minima of T_A - T_C for the 1st week of August 2008.

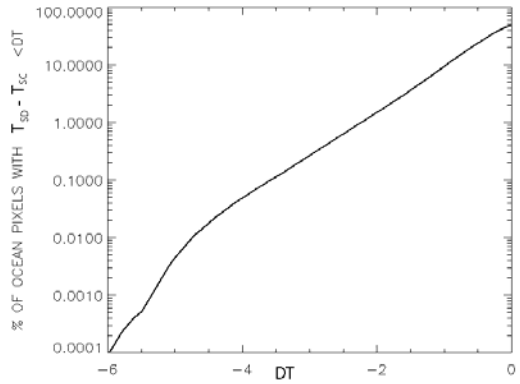

Fig. 6. The cumulative distribution of negative deviations of T_A from T_C.

5.2. *The ACM Spectral BT Test*

Spectral differences T_{3b} - T_5 (nighttime only) and T_4 - T_5 are known to be sensitive to the presence of clouds and are often used as cloud predictors. In CLAVRx the corresponding tests are called the "three minus five" test (TMFT) and "four minus five" test (FMFT). The ACM spectral BT test employs the FMFT during daytime and TMFT during nighttime. The thresholds for the ACM spectral tests were defined as maximum and minimum possible values of T_4 - T_5 and T_{3b} - T_5 for clear-sky conditions. These values were determined based on AQC classification of MetOp-A pixels for August 1 to 7, 2008 as functions of observed T_4 and satellite view zenith angle θ (Fig. 7).

The threshold conditions for the ACM spectral test are formulated as follows.

Nighttime:

$$T_4 - T_5 > \Delta T_{max\ night}(T_4, \theta) \text{ or } T_4 - T_5 < \Delta T_{min\ night}(T_4, \theta) ? \quad (7)$$

Daytime:

$$T_{3b} - T_5 > \Delta T_{max\ day}(T_4, \theta) \text{ or } T_{3b} - T_5 < \Delta T_{min\ day}(T_4, \theta) ? \quad (8)$$

If the corresponding condition is satisfied, then the pixel is "cloudy."

5.3. *The ACM Reflectance Tests*

ACM includes three daytime tests, whose predictors are derived from the observed reflectances in VIS and NIR channels: the reflectance gross contrast test (RGCT), the reflectance ratio contrast test (RRCT), and the channel 3 albedo test (C3AT). These tests were adopted from CLAVRx without changes. The test conditions for RGCT, RRCT, and C3AT are, respectively:

$$R_2 > T_{RGCT}(\theta,\theta_0,\varphi)? \text{ – if yes, the pixel is "cloudy"} \quad (9)$$

$$R_2/R_1 > T_{RRCT}(\theta,\theta_0,\varphi) ? \text{ – if yes, the pixel is "cloudy"} \quad (10)$$

$$R_{3a} > T_{C3aT}(\theta,\theta_0,\varphi)? \text{ – if yes, the pixel is "cloudy"} \quad (11)$$

R_1, R_2, and R_{3a} are observed reflectances in channels 1, 2, and 3a. The thresholds $T_{RGCT}(\theta,\theta_0,\varphi)$, $T_{RRCT}(\theta,\theta_0,\varphi)$, and $T_{C3aT}(\theta,\theta_0,\varphi)$ were precalculated using the 6S radiative transfer model (Vermote et al., 1997) for clear-sky atmosphere as functions of satellite view zenith angle θ, solar zenith angle θ_0, and solar azimuth φ.

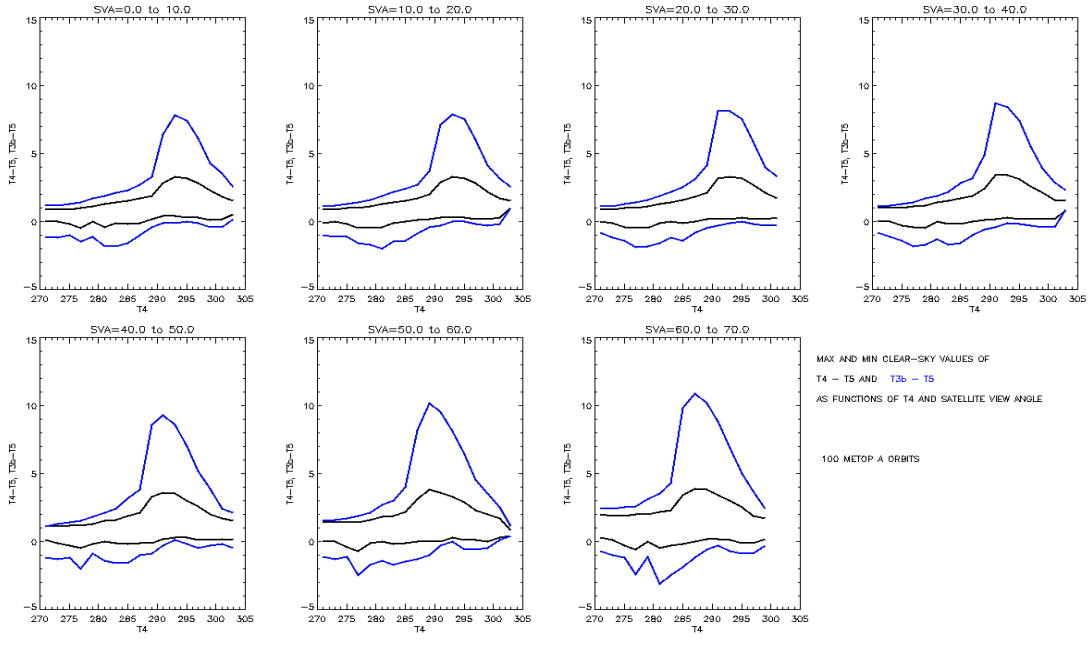

Fig. 7. The lower and upper thresholds for the differences T_4 - T_5 (black) and T_{3b} - T_5 (blue) in the ACM spectral BT test as functions of T_4 and the satellite view zenith angle (SVA).

5.4. *The ACM SST Uniformity Test*

Elevated spatial variability of observed BT or reflectances is often used as an indicator of semitransparent and fractional cloudiness. The implementation of this test in ACM was documented in Petrenko et al. (2008). First, ACM analyzes spatial variability of T_S rather than observed BT, which allows direct screening of residual cloud contaminations in the product. Second, special measures are taken to avoid false cloud detection, observed in the initial CLAVRx implementation over intensive ocean thermal fronts and coastal zones. The ACM uniformity test analyzes spatial variability of the difference T_S – median(T_S), where median(T_S) is the T_S field, passed through the median filter with 3 × 3 GAC pixels window. Since the median filter cuts off random noise and preserves regular contrasts (Gonzalez and Woods, 2003), the difference T_S – median(T_S) is more sensitive to random variations, typical for cloud effects, and much less sensitive to more regular surface contrasts caused by ocean thermal fronts.

6. THE AQC TESTS

The input for the AQC are "clear" and "probably clear" pixels, classified by the ACM. Some of the input pixels are reclassified as "cloudy" based on the AQC tests results.

The output of the AQC comprises the same three categories of pixels as the ACM. Only the "clear" category is recommended to the user. "Probably clear" pixels may be used for some other, less quantitative SST applications.

6.1 *The AQC SST Test*

The AQC SST test applies the logic described in Section 5.1 to the field of T_S anomalies with respect to T_A:

$$\Delta T_D = T_S - T_A - B_A \quad (12)$$

The condition for the initial pixel classification in the AQC SST test resembles one used in the ACM SST test:

$$\Delta T_A < \Delta T_{AQC\ SST}? \quad (13)$$

If yes, then the pixel is "cloudy". The difference from (4) is that the threshold $T_{AQC\ SST}$ is now location and time specific. $T_{AQC\ SST}$ is defined using the dynamic Estimated SST Error Standard Deviation σ_A (which is available from the Reynolds Daily SST data set) as follows:

$$\Delta T_{AQC\ SST} = \min(-5\sigma_A, -2K). \quad (14)$$

The values of σ_A typically vary from 0.1 K to 0.7 K, hence $\Delta T_{AQC\ SST}$ is close to -2 K for the most part of the world's oceans.

The adaptive part of the AQC SST test works similarly to that of the ACM SST test with the only difference being that ΔT_{CLOUD} and σ_{CLOUD} are now calculated through ΔT_A rather than ΔT_C, and

$$\sigma_{CLEAR} = \Delta T_{AQC\ SST}/3. \quad (15)$$

The size of a sliding window in the AQC SST test is 15 × 15 GAC pixels.

6.2. *The AQC Brightness Temperature Test*

The AQC BT test verifies accuracy of approximating the observed BTs using CRTM simulations with T_S and NCEP atmospheric water vapor forecast as input. In the current ACSPO version, the efficiency of this test is limited with accuracies of the regression T_S and the NCEP data. Nevertheless, this test was shown to improve the clear-sky statistics of observed BTs and, to a lesser extent, the accuracy of T_S (Petrenko et al., 2008, Liang et al., 2009). Currently the physical SST retrieval algorithm is under testing for the future ACSPO versions (e.g., Shabanov et al., 2009). This algorithm is expected to provide a better approximation of the observed BT under clear-sky conditions and to further enhance the performance of the BT test. The current test conditions in ACSPO are as follows:

Daytime:

$$[(T_4 - T_{4\ CRTM} + B_4)^2 + (T_5 - T_{5\ CRTM} + B_5)^2]/2 > \Delta T_{BT}? \quad (16)$$

- If yes, the pixel is "cloudy"

Nighttime:

$$[(T_{3b} - T_{3b\ CRTM} + B_{3b})^2 + (T_4 - T_{4\ CRTM} + B_4)^2 + (T_5 - T_{5\ CRTM} + B_5)2]/3 > \Delta T_{BT}? \quad (17)$$

- If yes, the pixel is "cloudy".

Here, $T_{3b\ CRTM}$, $T_{4\ CRTM}$ and $T_{5\ CRTM}$ are simulated BTs, B_{3b}, B_4 and B_5 are global biases of CRTM BT with respect to observed BT biases, which are estimated on-line similarly to the bias in T_S. The threshold ΔT_{BT} in (16) and (17) was set to $(1K)^2$ based on empirical considerations.

7. STATISTICS OF SST AFTER ACM AND AQC

In this section, the performance of the cloud filtering algorithms is preliminarily evaluated by the statistics of T_S - T_A for the pixels, classified as "clear" by the ACM and AQC.

Figs. 8 and 9 show histograms of T_S - T_A anomalies from August 1 to 7, 2008. The shapes of the histograms are close to a Gaussian and consistent for all platforms. The AQC handles the cold tail of the T_S anomalies much more efficiently. Table 1 shows summary statistics for the respective T_S - T_A distributions. The ratio of the amount of "clear" pixels to the total amount of ocean pixels varies from one platform to another and is typically from 17% to 23% for ACM and from 11.2% to 15% for AQC. The nighttime percent of "clear" pixels is greater for the morning platforms MetOp-A and NOAA-17 and smaller for the afternoon platforms NOAA-16 and NOAA-18. The cause for these systematic cross-platform differences is being investigated.

Variations in the mean anomaly biases between the platforms are generally consistent with variations in the

initial bias estimates B_A, shown on Fig. 3. Absolute bias values are slightly colder than B_A in the case of ACM and slightly warmer in the case of AQC. For ACM, the STDs of (T_S-T_A) are smaller in the daytime compared to nighttime. This difference is due to the remarkable work of the reflectance tests used in ACM. In AQC, the lack of reflectance tests in the nighttime is compensated by using a more accurate SST reference field and Ch3B in the BT test. As a result, for AQC the STDs of T_S anomalies are greater during the day than at night. Recall that variability in T_S is higher during daytime due to the effects of diurnal warming, which is globally non-uniform. Also, the nighttime three-channel MCSST algorithm (2) is more accurate than the daytime two-channel NLSST algorithm (1). In all cases (ACM and AQC, daytime and nighttime) the STDs of anomalies are consistent between all four platforms. The day- and nighttime AQC STDs of T_S anomaly are well within the 0.5 to 0.6 K range expected from comparison of satellite SSTs with *in situ* SSTs. It should be noted also that for ACM, the absolute value of the "gross" threshold, which cuts off unrealistic negative T_S anomalies, is approximately six times greater than the resulting STD of T_S clear-sky anomalies. For AQC, the "gross" threshold value is a factor of three to four times greater than the clear-sky STD. Hence, both in ACM and AQC the "gross" thresholds have little direct impact on the resulting T_S clear-sky anomalies distributions.

The negative skewness of the distributions after ACM is likely due to the effect of residual cloud. After the AQC, skewness is much closer to zero and even becomes slightly positive.

Figs. 10 and 11 show composite maps of T_S anomalies from August 1 to 7, 2008, produced from the MetOp-A pixels classified as "clear" by the ACM and AQC, respectively. The grid anomaly values were produced by averaging anomalies for all "clear" pixels within a given grid cell. The black color represents empty cells (i.e., those with no "clear" pixels). The ACM "clear" pixels show a better spatial coverage, but at a price of quite cold bias in T_S anomalies. On the other hand, the AQC leaves more data gaps, but the T_S anomalies in the remaining pixels show a much smaller bias.

8. SUMMARY AND FUTURE WORK

The two-step "telescopic" approach to filtering cloud effects within the ACSPO clear-sky products has been developed. Work is currently underway to implement this two-step cloud masking process in the subsequent ACSPO versions.

In the first step, the ACSPO cloud mask is produced using only static thresholds, which classifies all pixels into "clear", "probably clear", and "cloudy". Using static thresholds makes the cloud mask insensitive to the lack of external sources of real-time ancillary information.

In the second step, the ACM "clear" and "probably clear" pixels are additionally tested with more accurate quality control of clear-sky products using daily SST reference field, NCEP atmospheric temperature and water vapor forecast fields, and clear-sky radiative transfer simulations.

Preliminary evaluation of the ACM and AQC efficiency has been performed by comparison of retrieved SST with Reynolds daily SST product and evaluating the Gaussian statistics of the global anomaly. The AQC provides a superior statistics of the T_S field, whereas the ACM appears overly liberal and results in degraded-quality clear-sky products.

A large part of the suboptimal ACM performance is deemed to be due to using static climatological thresholds, which must be set liberally to avoid massive misclassification of "clear" pixels as "cloudy". Further optimization of the ACM and AQC thresholds will be explored to improve their performance.

Whatever the results of this optimization, integration of satellite radiances with global SST analysis and NWP forecast, in conjunction with using CRTM model, greatly improves the quality of the cloud masking in ACSPO. SST, estimated as a linear combination of BTs in TIR atmospheric transparency windows, used in conjunction with the reference SST fields, is a valuable cloud predictor used in both ACM and AQC. However, for the proper use of this predictor, it is important to account for real characteristics of T_S anomalies with respect to the reference SST field. The possible ways of correcting global biases of T_S anomalies and accounting for the accuracy of the SST reference fields are described in this paper.

Such bias correction, stratified by day/night and platform, is already in place in ACSPO v.1.10, which is currently being implemented into NESDIS operations. Future work will be aimed at improving satellite SST to minimize this bias and improve approximation of observed BT with simulations, based on T_S. The physical SST retrieval algorithm that was initially implemented in ACSPO shows promising results to improve the performance of the ACM and AQC. Further optimization of the bias estimation and correction will also be explored.

Our current results suggest that the global statistics of the number of clear-sky observations, SST bias, and STD are fairly comparable between day and night. However, the fact that the daytime and nighttime cloud screening and SST algorithms are not reconciled may lead to discontinuities at the day-night boundaries. Also, accuracy of cloud screening is degraded in the twilight zone around terminator. Work is underway to explore the daytime continuity of cloud mask and clear-sky products over ocean, and improve the quality of clear-sky products in the "gray area." This is particularly important for the analyses of geostationary products, which routinely progress through these situations twice daily.

ACKNOWLEDGEMENT

We thank our colleagues John Supper (NESDIS/OSDPD), Feng Xu (STAR/CIRA), Prasanjit Dash (STAR/CIRA) and Denise Frey (OSDPD/QSS) for helpful discussions and feedback.

This work is conducted under the Algorithm Working Group funded by the GOES-R Program Office. The views,

opinions, and findings contained in this report are those of the authors and should not be construed as an official NOAA or US Government position, policy, or decision.

REFERENCES

Ackerman, S.A., K.I. Strabala, W.P. Menzel, R.A. Frey, C.C. Moeller, and L.E. Gumley, 1998: Discriminating clear sky from clouds with MODIS, *J. Geophys. Res.*, **103**, 32,141–32,157.

Cayula, J.-F., and P. Cornillon, 1996: Cloud detection from a sequence of SST images. *Remote Sensing Environment*, **55**, 80–88.

Derrien, M. and H. Le Gleau, 2005: MSG/SEVIRI cloud mask and type from SAFNWC. *Int. J. Remote. Sensing*, **26**, No. 21, 4707–4732

Dybbroe, A., K.G. Karlsson and A. Thoss, 2005: NWCSAF AVHRR cloud detection and analysis using dynamic thresholds and radiative transfer modeling. Part I: Algorithm Description. *J. Appl. Met.*, **44**, 39–54.

Gonzalez, R.C., and R. E. Woods, 2003: *Digital image processing*. Pearson Education (Singapore) Pte. Ltd., Indian Branch.

Goodrum, G., K. Kidwell, and W. Winston (Eds.), 2003: *NOAA-KLM users guide*, U.S.Dept. Of Commerce, NOAA/NESDIS. (Available from NCDC, 151 Patton Ave, Rm.120, Asheville, NC 28801-5001).

Heidinger, A., V.R. Anne, and C. Dean, 2002: Using MODIS to estimate cloud contamination of the AVHRR data record. *J. Atmos. Ocean. Technology*, **19**, 586–601.

Heidinger A., 2004: CLAVR cloud mask algorithm theoretical basis document, NOAA/NESDIS Center for Satellite Applications and Research.

Han Y., P. van Delst, Q. Liu, F. Weng, B. Yan, and J. Derber, 2005: User's guide to the JCSDA Community Radiative Transfer Model (Beta Version), NOAA/NASA JCSDA, http://www.star.nesdis.noaa.gov/smcd/spb/CRTM/crtm-code/CRTM_UserGuide-beta.pdf.

Ignatov, I., J. Supper, I. Laszlo, et al, 2004: Global operational SST and aerosol products from AVHRR: current status, diagnostics, and potential enhancements. 13th AMS Conference on Satellite Meteorology and Oceanography, Norfolk, VA, 20–23 September 2004.

Liang, X., A. Ignatov, and Y. Kihai, 2009: Implementation of the Community Radiative Transfer Model (CRTM) in AVHRR Clear-Sky Processor for Oceans (ACSPO) and validation against nighttime radiances. *JGR, submitted.*

Kriebel, K.T., G. Gesell, M. Kastner, and H. Mannstein, 2003: The cloud analysis tool APOLLO: improvements and validation. *Int. J. Remote Sensing*, **24**, 2389–2408.

Martins, J.V., D. Tanre, L. Remer, Y. Kaufman, S. Mattoo, and R. Levy, 2002: MODIS cloud screening for remote sensing of aerosols over oceans using spatial variability. *Geophys. Res. Letters*, **29**, MOD4-1 – MOD4-4.

McClain, E.P., W.G. Pichet, and C.C. Walton, 1985: Comparative performance of AVHRR-based multichannel sea-surface temperatures. *J. Geophys. Res.*, 90, 1587–1601.

Minnis P., Q.Z. Trepte, S. Sun-Mack, Y. Chen, D.R. Doelling, D.F. Young, D.A. Spangenberg, W.F. Miller, B.A. Wielicki, R.R. Brown, S.C. Gibson, and E.B. Geier, 2008: Cloud detection in non-polar regions for CERES using TRMM VIRS and Terra and AQUA MODIS data. *IEEE TGARS*, in press.

Pellegrini, P.F., M. Bocci, M. Tommasini, and M. Innocenti, 2006: Monthly averages of sea surface temperature. *Int. J. Remote Sensing*, **27**, 2519–2539.

Petrenko, B., A. Ignatov, Y. Kihai, and A. Heidinger, 2008: Clear-sky mask for the AVHRR Clear-Sky Processor for Oceans. Ocean Science Meeting, 2–7 March 2008, Orlando, FL, http://www.star.nesdis.noaa.gov/smcd/emb/aerosol/ignatov/conf/2008-AGU-OSM-PetrenkoEtAl_ACSPO_CSM_Poster.pdf

Reynolds, R.W., N.A. Rayner, T.M. Smith, D.C. Stokes, and W. Wang, 2002: An improved in situ and satellite SST analysis for climate. *J. Climate*, 16, 1495–1510.

Reynolds, R.W., T.M. Smith, C. Liu, D.B. Chelton, K.S. Casey, and M.G. Schlax, 2007: Daily high-resolution-blended analyses for sea surface temperature. *J. of Climate*, **20**, 5473–5496

Saunders, R.W. and K.T. Kriebel, 1988: An improved method for detecting clear sky and cloudy radiances from AVHRR data. *Int. Journal Remote Sensing*, **9**, 123–150.

Shabanov, N., A. Ignatov, B. Petrenko, Y. Kihai, X. Liang, W. Guo, F. Xu, P. Dash, M. Goldberg, and J. Sapper, 2009: Prototyping SST retrievals from GOES-R ABI with MSG SEVIRI data, Fifth Annual Symposium on Future Operational Environmental Satellite Systems-NPOESS and GOES-R (submitted).

Stowe L.L., P.A. Davis, and E.P. McClain, 1999: Scientific basis and initial evaluation of the CLAVR-1 global clear/cloud classification algorithm for the Advanced Very High Resolution Radiometer. *J. Atmos. Ocean. Technology*, **16**, 656–681.

Vermote, E., D. Tanre, J. L.Deuze, M. Herman and J.J. Morcrette, 1997: Second simulation of the satellite signal in the solar spectrum, 6S: an overview, *IEEE Trans. Geosci. Remote Sens*. **35**, 675–686.

Xue, Y., T.M. Smith, and R.W. Reynolds, 2003: Interdecadal changes of 30-year SST normals during 1871-2000. *Int. J. Climate*, **16**, 1601–1612

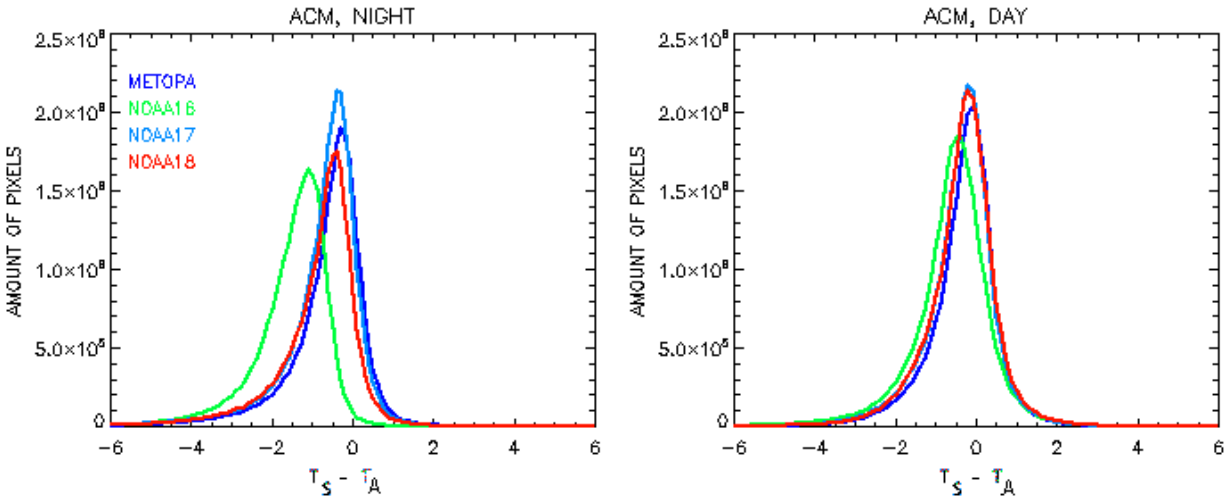

Fig. 8. Histograms of T_S - T_A anomalies over pixels, "clear" by ACM for four platforms, carrying AVHRR instruments.

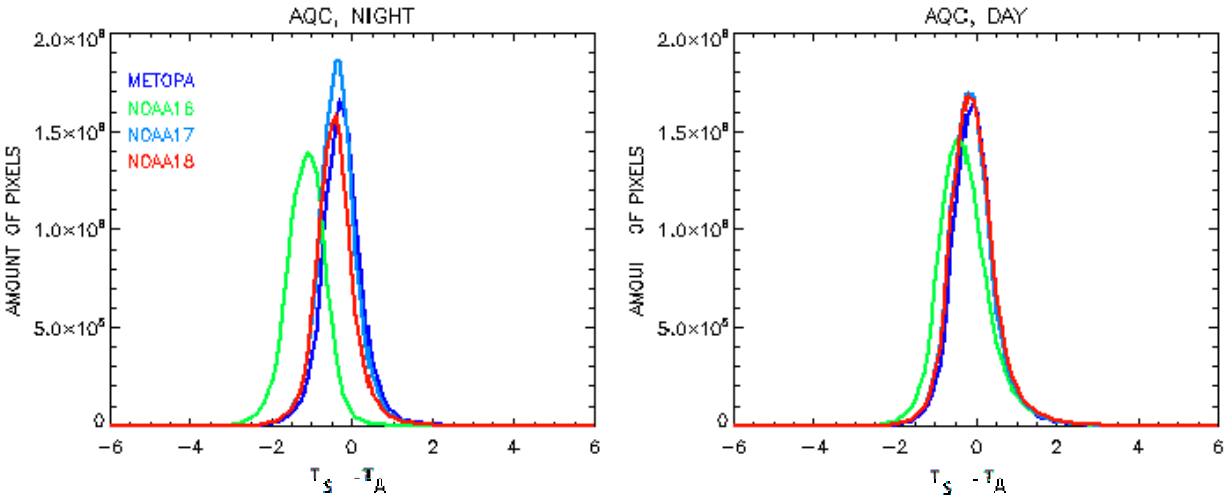

Fig. 9. Histograms of T_S - T_A anomalies over pixels, "clear" by AQC for four platforms.

Table 1. Statistics of T_S - T_A anomalies for "clear" pixels after ACM and AQC for four platforms

Platform	Percentage of "clear" pixels to the total amount of ocean pixels, %	Mean, K	STD, K	Skewness	Kurtosis
ACM-Night					
MetOp-A	22.3	-0.52	0.97	-1.63	5.41
NOAA-16	17.8	-1.41	0.92	-1.39	3.87
NOAA-17	22.1	-0.65	1.00	-1.81	6.02
NOAA-18	19.8	-0.77	1.04	-1.68	5.56
ACM-Day					
MetOp-A	22.0	-0.22	0.86	-0.83	4.32
NOAA-16	23.0	-0.51	0.99	-0.86	3.89
NOAA-17	22.4	-0.30	0.89	-0.80	4.22
NOAA-18	21.3	-0.27	0.91	-0.81	5.81
AQC-Night					
MetOp-A	14.8	-0.14	0.52	0.52	3.61
NOAA-16	11.2	-1.02	0.50	0.20	3.01
NOAA-17	14.6	-0.24	0.50	0.46	3.76
NOAA-18	12.9	-0.31	0.51	0.61	4.21
AQC-Day					
MetOp-A	14.5	0.07	0.58	1.02	5.60
NOAA-16	15.0	-0.17	0.67	0.94	3.53
NOAA-17	14.4	0.02	0.61	1.12	5.52
NOAA-18	13.7	0.06	0.63	1.28	7.00

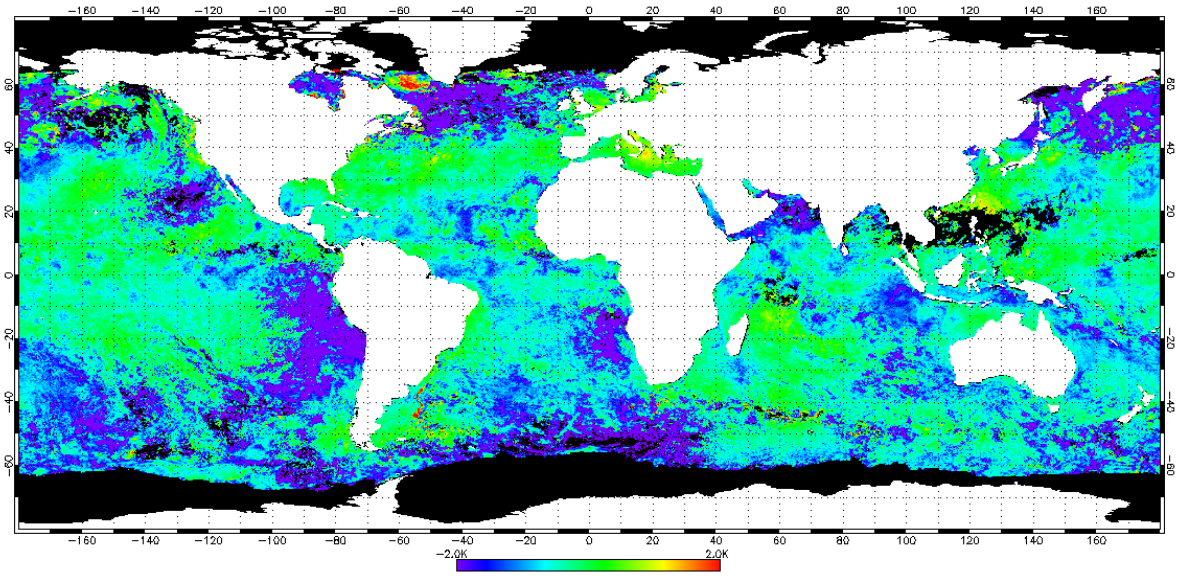

Fig. 10. A composite map of T_S - T_A anomalies produced from ACM "clear" pixels from nighttime measurements on the MetOp-A satellite from August 1 to 7, 2008.

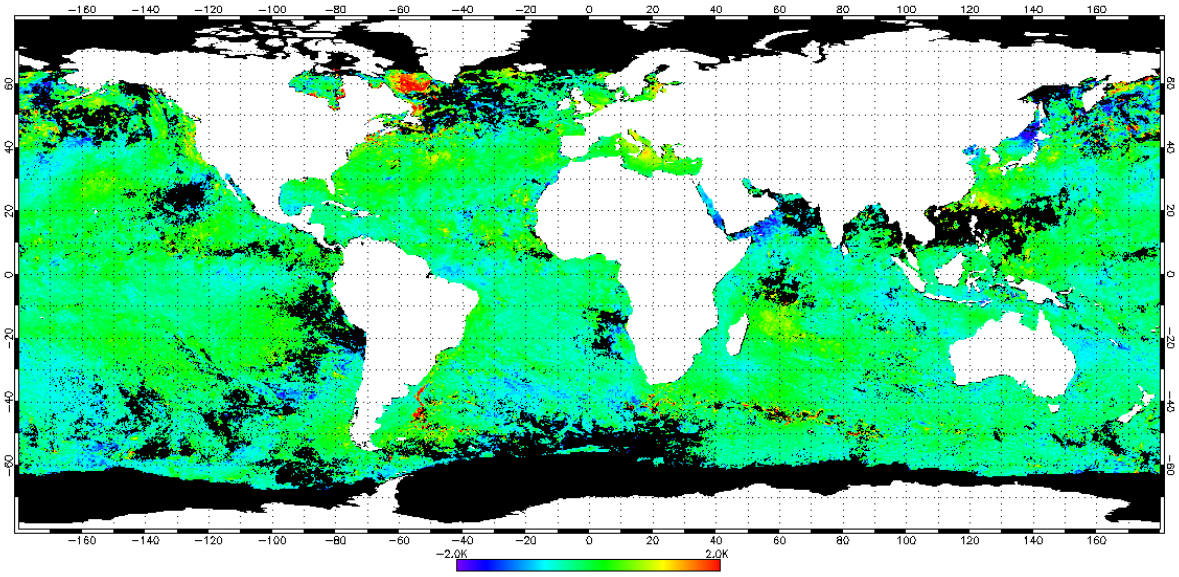

Fig. 11. A composite map of T_S - T_A anomalies produced from AQC "clear" pixels from nighttime measurements on the MetOp-A satellite from August 1 to 7, 2008.